The Fringe Detection Laser Metrology for the GRAVITY Interferometer at the VLTI

H. Bartko[a], S. Gillessen[a], S. Rabien[a], M. Thiel[a], A. Gräter[a], M. Haug[a], S. Kellner[a], F. Eisenhauer[a], S. Lacour[b], C. Straubmeier[c], J.-P. Berger[d,e], L. Jocou[d], W. Chibani[a], S. Lüst[a], D. Moch[a], O. Pfuhl[a], W. Fabian[a], C. Araujo-Hauck[c], K. Perraut[d], W. Brandner[f], G. Perrin[b], A. Amorim[g]

[a] Max-Planck-Institute for Extraterrestrial Physics, Garching, Germany;
[b] LESIA, UMR 8109, Observatoire de Paris, CNRS, UPMC, Université Paris Diderot, 92190 Meudon, France; Groupement d'Intérêt Scientifique PHASE (Partenariat Haute résolution Angulaire Sol Espace) between ONERA, Observatoire de Paris, CNRS and Université Paris Diderot;
[c] I. Physikalisches Institut, Universität zu Köln, 50937 Köln, Germany;
[d] Laboratoire d'Astrophysique, Observatoire de Grenoble, 38041 Grenoble Cédex 9, Frances;
[e] ESO, Garching, Germany;
[f] Max-Planck-Institut für Astronomie, 69117 Heidelberg, Germany;
[g] SIM, Faculdade de Ciencias da Universidade de Lisboa, Portugal.

ABSTRACT

Interferometric measurements of optical path length differences of stars over large baselines can deliver extremely accurate astrometric data. The interferometer GRAVITY will simultaneously measure two objects in the field of view of the Very Large Telescope Interferometer (VLTI) of the European Southern Observatory (ESO) and determine their angular separation to a precision of 10 μas in only 5 minutes. To perform the astrometric measurement with such a high accuracy, the differential path length through the VLTI and the instrument has to be measured (and tracked since Earth's rotation will permanently change it) by a laser metrology to an even higher level of accuracy (corresponding to 1 nm in 3 minutes). Usually, heterodyne differential path techniques are used for nanometer precision measurements, but with these methods it is difficult to track the full beam size and to follow the light path up to the primary mirror of the telescope. Here, we present the preliminary design of a differential path metrology system, developed within the GRAVITY project. It measures the instrumental differential path over the full pupil size and up to the entrance pupil location. The differential phase is measured by detecting the laser fringe pattern both on the telescopes' secondary mirrors as well as after reflection at the primary mirror. Based on our proposed design we evaluate the phase measurement accuracy based on a full budget of possible statistical and systematic errors. We show that this metrology design fulfills the high precision requirement of GRAVITY.

Keywords: Astrometry, Interferometry, Metrology, VLTI.

1. INTRODUCTION

Interferometric measurements of path length differences of stars over large baselines can deliver extremely accurate astrometric data, which is one of the motivations to build an astronomical interferometer. The interferometer GRAVITY will be capable of detecting two objects simultaneously in the field of view of the VLTI. Both objects are separated at the VLTI interferometric laboratory within the instrument and detected in separate beam combiners. To perform the astrometric measurement with high accuracy, the differential path length through the VLTI and the instrument has to be known (and tracked since Earth's rotation will permanently change it) at an even higher level of accuracy. This is the scope of a dedicated system, commonly called metrology. The error

Send correspondence to H. Bartko (E-mail: hbartko@mpe.mpg.de)

budget of the whole instrument leaves an RMS dOPD (differential optical path difference) error of 1 nm within a total of 3 min integration time for the metrology (see Gillessen et al.[1] 2010). The difference in path length occurs primarily within the instrument after the field separation. But a difference in path length can also occur within the VLTI, since the traveled path depends on the exact footprint of the beam through the VLTI optics. Special points where large systematic differences can occur are at the field locations, where optical elements are present. The variable curvature mirror (VCM) with ∼150 nm surface variation due to adaption of the surface shape is among the candidates to introduce large field dependent path length changes in a systematic way. Thus an active measurement of the path length within the instrument and the VLTI is required. The PRIMA facility uses a heterodyne difference frequency technique with lasers launched at the center of the pupil at the beam combiner and being back reflected from a retro reflector behind the MACAO dichroic mirror (Leveque et al.[2] 2003). The quantity measured is the optical path length difference for each object between the two telescopes from the beam combiner to the dichroic mirror. On the one hand, the difference frequency technique is known to be extremely accurate and laser intensity independent. On the other hand, the center of pupil measurement does not trace the path of the science light, since soon after leaving the pupil plane the two beams begin to travel along different paths and measuring the center of the beams will not represent the complete truth. In particular, in a focal plane the small laser beam will form a larger PSF than the science light does. The preliminary design of the GRAVITY metrology follows an implementation which (Rabien et al.[3] 2008):

- maps the full pupil with the metrology beams
- covers the total length of the instrument and the VLTI up to the entrance pupil of the system, the secondary mirror of the VLT telescopes
- allows a measurement for all beams in parallel
- requires only minor retro fittings of the VLTI or VLTs.

The basic idea is to split a laser beam into two equally bright beams with a fixed phase relation and inject them backwards into the two beam combiners. From both beam combiners four beams will then travel the exact same path backwards through the instrument and VLTI as the science light is traveling forward. At the VLT secondary, the entrance pupil of the system, the laser beams from the two beam combiners will interfere and form a fringe pattern. This fringe pattern will be detected with an off-axis infrared camera in the scattered light from the UTs secondary mirror plus dedicated scattering screens attached to the telescope spider holding the secondary mirror. The interferogram can finally be used to determine the differential path up to this point. This concept is illustrated in Figure 1.

2. PHYSICAL REQUIREMENTS ON GRAVITY METROLOGY

2.1 Accuracy of Phase Measurements

The required accuracy for the metrology measurement is driven by three factors:

- The measurements of the stellar phase differences should be the main contributors to the astrometric error budget; the metrology error should only contribute marginally: 1 nm dOPD error in 3 minutes
- The metrology signal shall allow the differential delay lines (DDL) loop to be stably closed: maximum phase error per ABCD 0.13 rad, see section 7.2.
- The metrology needs to be fast enough to drive the phase at a reasonable speed during the acquisition procedure.

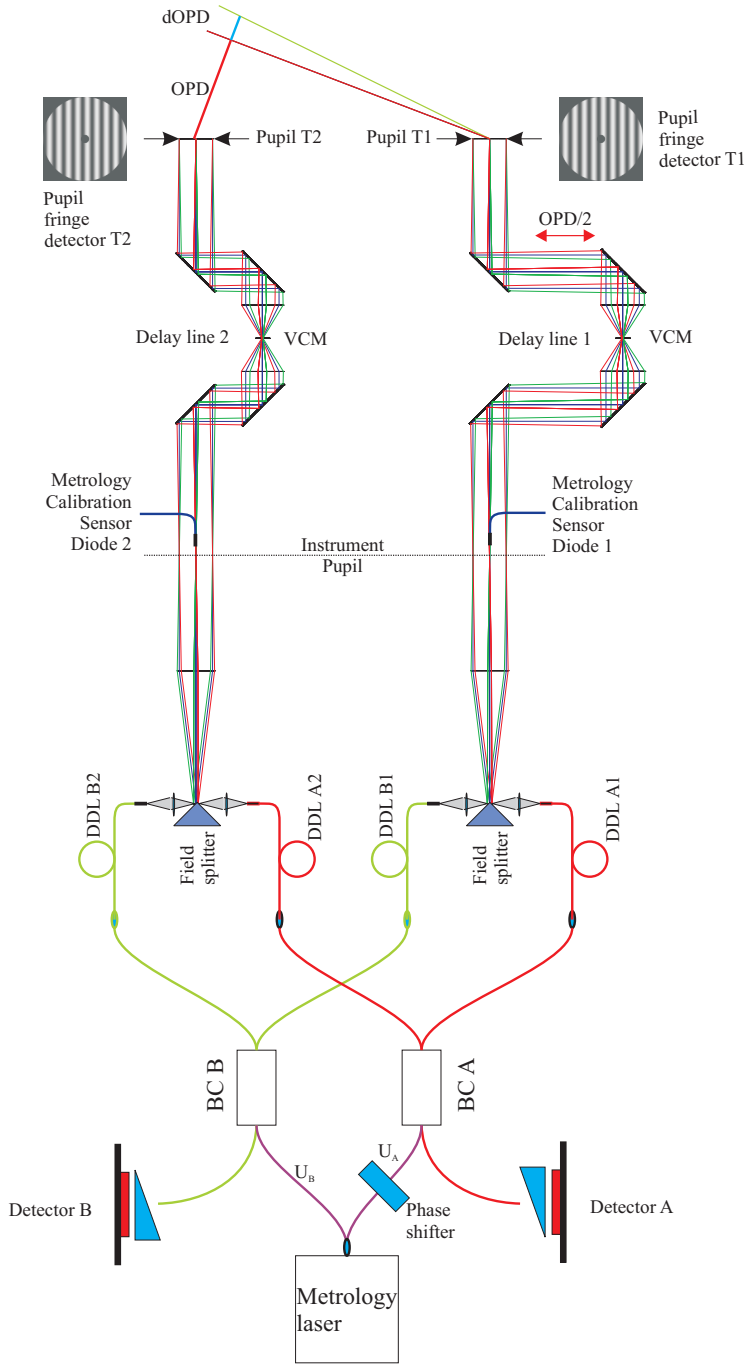

Figure 1. Principle of the GRAVITY metrology system shown for two telescopes. A laser beam travels the same path backwards through all the beam combination and the VLTI optical train. Detection of the resulting fringe pattern takes place by imaging the VLT secondary mirror plus dedicated scattering screens on the telescope spider with an off-axis infrared camera.

2.2 Metrology Fringe Detection in M1 Space

As shown by Lacour et al.[4] (2010), the narrow angle baseline for the astrometric mode of GRAVITY is defined by the vector between the two points (projected to M1 space if not defined therein) on each telescope where the

metrology phase measurement is made. This requires a metrology fringe detection after reflection on M1 at a fixed position with respect to M1.

For both UTs and ATs we will sample the metrology interference pattern after reflection on M1 with dedicated scattering screens / photo diodes, which have fixed positions with respect to M1 on the M2/M3 spider arms. We use their signals to compute the metrology phase in real-time. All individual phase measurements will be weighted and averaged to obtain a single phase measurement per telescope.

In our current baseline design, as presented in this document, we plan to record full images of the fringe pattern on M2 with IR cameras in scattered light for the UTs. This data will enable us to correct off-line for possible higher order aberrations (Rabien et al.[3] 2008). In August 2010 we will conduct a Metrology test at the ESO Paranal observatory to measure the amount of quasi-static differential abberations, and their stability. In case of sufficiently small and stable abberations, it may be sufficient to only sample the metrology fringe pattern with diodes also in the case of the UTs.

3. METROLOGY SYSTEM DESIGN

3.1 Basis Description of Working Principle

Figure 1 shows a schematic drawing of the optical path within the VLTI and the GRAVITY instrument. The light from two astronomical objects enters the system at the telescope pupils, e.g. the VLT secondary mirrors. The brighter of the two objects (A) is marked in red, the other one (B) in green. The optical path length difference to the beam combination has to be compensated for with the VLTI main delay lines. Within the instrument the light from the two objects is separated at the field splitter and sent through differential delay lines (DDLs) to the beam combination (BC A and BC B), after which the light is fed into the spectrometers. A laser source operating at 1908 nm near the atmospheric K band is split into two beams and sent backwards into the beam combiners. Starting at the beam combiner, the laser light travels exactly the same path backwards through the VLTI, as the light from objects A and B travels forward. At each pupil the laser wavefronts overlap, tilted by an angle with respect to each other that corresponds to the angular separation of the astronomical objects A and B, and create interference fringes. The maximum number of fringes for a 2" UT field of view (FOV) and a metrology wavelength of 1908 nm is 40.5 fringes. These fringes can be detected in scattered light from the secondary mirror, as well as from dedicated scattering screens mounted on the telescope spider, with an off-axis infrared camera, or directly using infrared sensitive photodiodes. The following analysis of the optical path length differences along the science and the metrology beams shows that the proposed setup is able to deliver the desired differential dOPD from the measurements on sky and from the fringe pattern detected on the telescopes. The individual optical path lengths through the system are denoted as:

L_{A1}	red path from the telescope T1 to the DDLA1
L_{A2}	red path from the telescope T2 to the DDLA2
L_{B1}	green path from the telescope T1 to the DDLB1
L_{B2}	green path from the telescope T2 to the DDLB2
DL_{xx}	path length from the differential delay line entrance up to the beam combination
U_A , U_B	path lengths from the metrology laser splitter to the beam combiners.

The following four quantities Ψ_A, Ψ_B, Φ_A and Φ_B are measured: Ψ_A is the phase difference of the light of star A with an effective wavelength λ_A measured at detector A (for the definition and measurement of effective wavelength see Choquet et al.[5] 2010):

$$\Psi_A = \{(L_{A1} + DL_{A1}) - (L_{A2} + DL_{A2} + OPD)\} \frac{2\pi}{\lambda_A} . \quad (1)$$

Ψ_B is the corresponding phase difference of the light of star B measured at detector B. Since the phases of the stars' light will be measured for multiple wavelengths, an absolute length difference can be detected, e.g. the center of the white light fringe can be determined at the point where $\Psi_A = 0$ for all λ_i (see Choquet et al.[5]

2010). In contrast to that, the phase difference for the single metrology laser wavelength is only unambiguous within the interval $-\pi < \Phi < \pi$. At the laser fringe detector at telescope number 1 the phase difference of the laser beams for the laser wavelength λ_L is:

$$\Phi_1 = \{(L_{A1} + DL_{A1} + U_A) - (L_{B1} + DL_{B1} + U_B)\} \frac{2\pi}{\lambda_L} + n_1 2\pi = \{(L_{A1} + DL_{A1}) - (L_{B1} + DL_{B1})\} \frac{2\pi}{\lambda_L} + \Delta_1 \ , \tag{2}$$

similar at the laser fringe detector number 2:

$$\Phi_2 = \{(L_{A2} + DL_{A2} + U_A) - (L_{B2} + DL_{B2} + U_B)\} \frac{2\pi}{\lambda_L} + n_2 2\pi = \{(L_{A2} + DL_{A2}) - (L_{B2} + DL_{B2})\} \frac{2\pi}{\lambda_L} + \Delta_2 \ . \tag{3}$$

The constants Δ_1 and Δ_2 can be determined with the metrology zero point calibration procedure, see section 6.2. In the astrometric mode of GRAVITY the quantity that has to be measured is dOPD on sky:

$$\text{dOPD} = \Psi_A \frac{\lambda_A}{2\pi} - \Psi_B \frac{\lambda_B}{2\pi} + (\Phi_2 - \Phi_1)\frac{\lambda_L}{2\pi} - (\Delta_2 - \Delta_1)\frac{\lambda_L}{2\pi} \ . \tag{4}$$

This equation contains only the measurable quantities and the calibration phases. It shows that the quantity dOPD can be retrieved from the beam combiners and the metrology signals. Each of the values above contributes to the final error budget.

3.2 Phase Shifting Interferometer

The laser wavefronts that are launched from the fiber exits will overlap in the pupil plane of the telescopes. From the resulting intensity distribution the global phase offset has to be extracted. The intensity distribution is detected with a camera which images the scattered light from the secondary mirror and dedicated scattering screens installed on the telescope spiders. The phase extraction from these images has to solve for the following properties:

- Most likely the intensity distribution, even if being emitted perfectly Gaussian from the fibers, will not be smooth and Gaussian any more after having passed all the VLTI beam train.
- The scattering process from the solid surface and dust particles will result in a speckle pattern on the camera, due to the coherence of the light and the surface inhomogeneities.
- The intensity of the scattered light at the secondary mirrors will be low, since it is a high quality mirror.
- There will be background radiation, since the ambient temperature is 280K.
- The intensity pattern will rotate with the field rotation on sky.
- During the calibration process the number of fringes in the pupil plane will vary between 0 and 40 for a maximum separation of the objects of 2" (UTs).
- The phase computation must be sufficiently fast to steer the differential delay lines (see section 6.2).

To meet these requirements the proposed method for the phase extraction follows a routine based on phase shifting interferometry. Widely used for the measurement of optical surfaces, phase shifting interferometry (PSI) allows a phase difference to be measured with high accuracy. Standard laboratory interferometers make use of the comparison between a reference phase and a phase under test, e.g. in a Twyman-Green setup. The reference beam is phase shifted in several steps, and an interferogram is recorded at each step. Due to the coherence of the laser wavefronts, the intensity at each position (x, y) follows the equation of a two-beam interference:

$$I(x, y, \alpha) = I'(x, y) + I''(x, y) \cos(\Phi(x, y) + \alpha) \ . \tag{5}$$

Here, α is the global additional phase difference, which is deterministically added to the launched beam. There are several standard algorithms to calculate the local phase from a set of phase shifted interferograms, which can

be found in textbooks (e.g. Malacara[6] 1992). With the four-step algorithm four interferograms are recorded with phaseshifts of $\alpha_i = 0, \pi/2, \pi, 3\pi/2$ respectively. The solution to the four equations contains only the measured intensities:

$$\tan(\Phi(x,y)) = \frac{I_4 - I_2}{I_1 - I_3} \ . \tag{6}$$

Comparable solutions can be found for three or more steps, e.g. the Hariharan or Carré algorithm. Since we are only interested in a global phase difference from the calibration point to the observation location in the field, an absolute phase measurement is not needed, and the observed 2π jumps can be recorded in a counter. The ABCD algorithm allows a relatively simple and straight forward calibration of the phase shifter to the values even for a non-linear phase shift response of the phase shifter to the control voltage, see section 6.1.2.

4. HARDWARE

In this section we will describe the preliminary design and layout of the hardware of the GRAVITY metrology. The analysis of the performance of the full GRAVITY metrology system based on the hardware requirements will be presented in section 7.

4.1 Hardware Overview

Figure 2 shows a sketch of the metrology hardware: The hardware of the metrology system located in or near the VLTI laboratory includes the metrology laser source, the beam transmission fiber, the splitting and phase shifting unit and the metrology fiber positioner for the coupling adjustment of the IR laser light into the IO via the spectrometer optics. The laser itself with the frequency control unit will be located in the GRAVITY electronics racks in the Combined Coudé lab. The laser foreseen will be a commercial high power single frequency laser. The delivery of the laser light to the GRAVITY beam combiner instrument will be done with a single mode polarization maintaining fiber. Since the phase of the laser in front of the cryostat is unimportant, the fiber delivery needs no special protection. The fiber is connected to the inside of the cryostat by a commercially available single mode and polarization maintaining fiber feed-through.

In the cryostat the laser will be split into four beams with equal intensity. Two of the arms are directed to electro-optical phase shifters. After the phase shifting the four fibers are routed to the metrology fiber positioners, which align the fibers in the field before the fiber coupling optics of the spectrometer (Araujo-Hauck et al.[7] 2010, Straubmeier et al.[8] 2010). The alignment is motorized in three axes for each fiber to allow a remote coupling efficiency optimization, while the cryostat is closed. After the light leaves the fibers, it is collimated at the laser collimator in the spectrometer and joins the science light at a dichroic beam splitter and is injected into the waveguide of the integrated optics (IO, Jocou et al.[9] 2010).

The metrology light passes the integrated optics backwards, in the opposite direction of the starlight. Inside the IO the metrology light is split such that all four entrance fibers of the IO contain equal amounts of metrology light. The metrology light travels trough the fiber control units containing the differential delay lines (DDLs) and polarization rotators (see Perrin et al.[10] 2010) to the field splitter of the GRAVITY fiber coupler (see figure 4). In the field splitter the metrology light from the beam combiners A and B is Combined and via the VLTI optical train guided to the four telescopes. As the laser light from the two beam combiners A and B is coherent, there is a characteristic interference pattern in each instrument pupil. The number of fringes visible in the instrument pupil depends on the angular separation of the fibers in the fiber coupler projected on the sky. The 2" maximum field of view of the VLTI (UTs) corresponds to 40 interference fringes.

For the GRAVITY metrology two instrument pupils are of special importance: first, the pupil in the GRAVITY fiber coupler (Pfuhl et al.[11] 2010). The interference pattern in this pupil is sampled by the metrology calibration sensor diode and allows an accurate calibration and monitoring of the active components like the metrology laser, phase shifter and fiber controllers. Second, there is also the characteristic interference pattern of the metrology laser light visible at the entrance pupil of the telescopes, M2. In case of the UTs the full M2 pupil will be imaged in scattered light, plus dedicated scattering screens on the M2 spider. In case of the ATs the pupil will be sampled with photodiodes mounted on the M3 spider.

In the following we will detail the hardware items and specify their performance requirements.

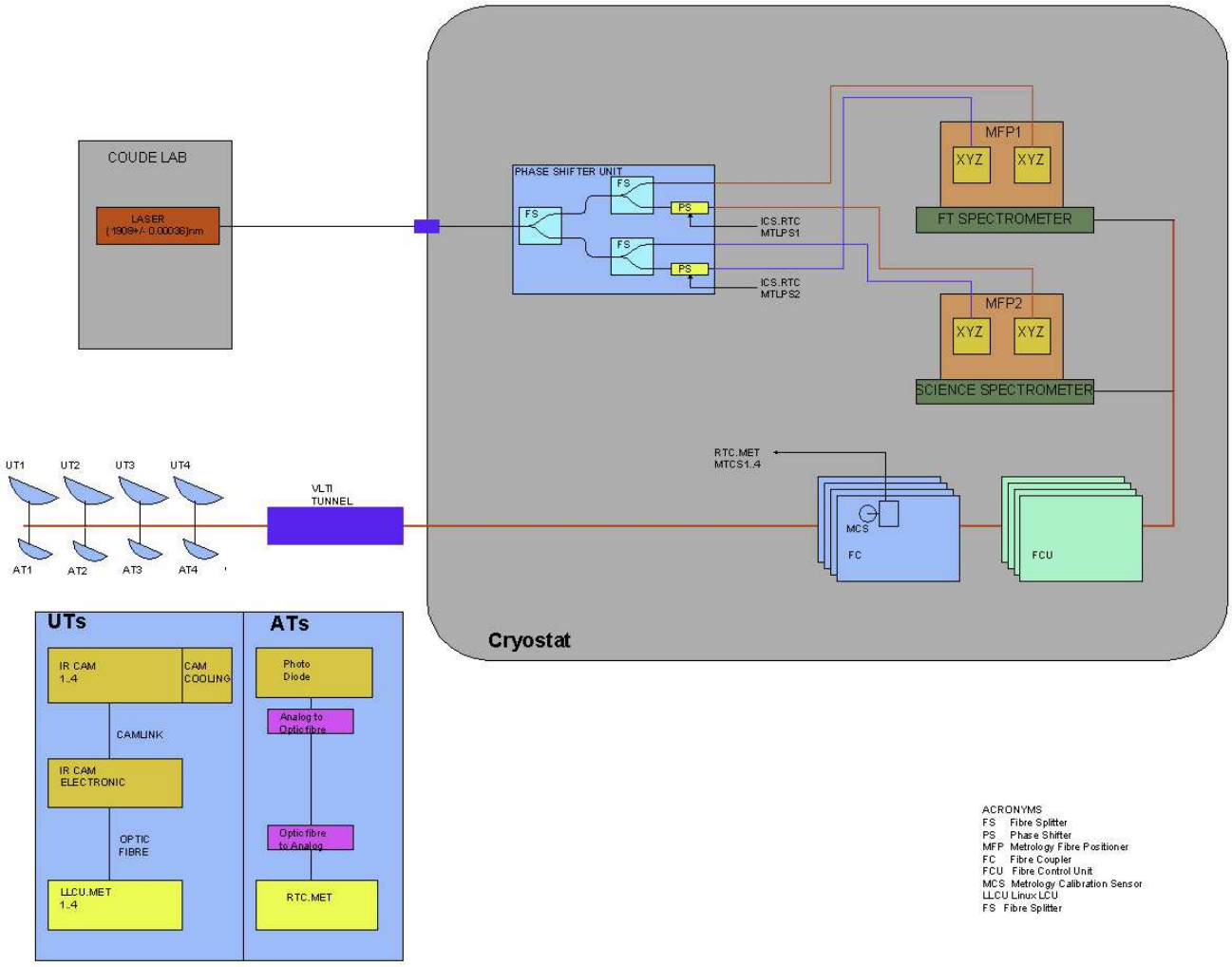

Figure 2. Sketch of the metrology hardware. The metrology laser system is located in the electronics racks of the Combined Coudé laboratory. The metrology laser light is sent via a single mode polarization maintaining fiber to the GRAVITY cryostat. In the cryostat a splitting and phase shifting unit is located. The laser is first split in two steps into four fibers containing equal amounts of light. Two of the fibers pass an electro-optical phase shifter before they are directed to the metrology fiber positioners. The two other fibers are directly routed to the fiber positioner. The fibers end at the interface between the metrology fiber positioner and the cryostat. The metrology light enters the laser collimation optics of the spectrometer as a free beam. It is directed towards the IO beam combiner and overlayed onto the stellar light with a dichroic beam splitter. Finally, the metrology laser light is fed into two of the 24 exits of the integrated optics. In the IO the laser light is split again and distributed to the four entrance fibers of the IO beam combiners. The interference pattern in the pupil of the Fiber Coupler is sampled by the metrology calibration sensor diode and allows an accurate calibration and monitoring of the active components like the metrology laser, phase shifter and fiber controllers. A characteristic interference pattern of the metrology laser light will be visible at the entrance pupil of the telescopes, M2. In case of the UTs the full M2 pupil will be imaged in scattered light, plus dedicated scattering screens on the M2 spider. In case of the ATs the pupil will be sampled with photodiodes mounted on the M3 spider.

4.2 IR Laser System

The metrology laser system shall produce high power single frequency laser light coupled inside a single mode polarization maintaining fiber. The stability of the laser frequency as well as the laser power is of special concern. The proposed laser system shall fulfill the following requirements:

- power output: > 2W continuous wave
- single frequency laser with output wavelength: (1908 ± 1) nm, stabilized to ± 30 MHz absolute wavelength accuracy
- linear polarized
- power output fluctuations: $< 0.5\%$ RMS of the integrated laser power over a 33 ms timescale.

4.3 Passive Fiber Optic Components

The polarization maintaining fibers transport the laser light from the laser source to the metrology fiber positioner units. The fiber path from the metrology laser splitter to the beam combiner, $U_{A/B}$ is of special importance. It is a so-called non-common path, where the laser light does not follow the star light. The path length difference $\Delta_2 - \Delta_1$ (see equation 4 and section 4) can be calibrated, see equation 10 and section 6.2, but needs to be stable at a level below 0.5 nm during the observation (see section 7.4). The optical path length of an optical fiber changes (ΔL) as a function of temperature change (ΔT):

$$\Delta L = (n\alpha + \mathrm{d}n/\mathrm{d}T) l \Delta T \ , \tag{7}$$

where α denotes the linear thermal expansion coefficient, n the index of refraction and l is the fiber length. Standard fused silica fibers show an optical path length change of: $\Delta L = 1\mathrm{nm}(\Delta T/10\mathrm{mK})(l/1\mathrm{cm})$ (Leviton & Frey[12] 2006). Air-guiding photonic-bandgap fibers offer much smaller path length differences (Dangui et al.[13] 2005).

4.4 Phase Shifter

The two phase shifters provide the phase shifts of $\alpha_i = 0, \pi/2, \pi, 3\pi/2$ necessary for the ABCD phase shifting interferometer algorithm. For this a very accurate reproducibility of the phase shifts is of utmost importance. The phase shifters are commercially available as integrated optics components employing LiNbO3 crystals. By applying an appropriate voltage to the birefringent crystal a corresponding change in the extraordinary refractive index will occur. If the optical input is both linearly polarized and aligned with the extraordinary axis of the modulator crystal, the output will undergo a pure phase shift with no change in the state of polarization. The phase shifters shall fulfill the following requirements:

- transmission $> 70\%$, full-wave amplitude modulation $< 0.5\%$
- phase shifting repeatability $< \lambda/5000$
- operation laser power: 0.5 W, damage threshold > 1 W
- min. 13 effective bits, absolute voltage repeatability $< 1/5000$.

4.5 Metrology Calibration Sensor Diode

The metrology Calibration Sensor Diode samples the light flux in the center of the 18 mm diameter pupil in the Fiber Coupler subsystem (see figure 4). This allows to (see also section 6.1):

- adjust/monitor the metrology fiber positioner
- monitor the laser power
- in-situ calibrate the phase shifter
- calibrate the DDL, monitor the DDL position.

Requirements:

- pick-up fiber with core diameter: 100...110 μm, total transmission T$> 90\%$
- combined diode and amplifier responsivity: $8{\cdot}10^{-9}$ W shall be converted to 10 V, bandwidth (3dB) 1000 Hz, input current equivalent noise: $< 3 \cdot 10^{-12}$ A / Hz$^{1/2}$, maximum non-linearity for 10 V output of $< 0.1\%$
- ADC sampling rate $\geq$ 1kS/s, min. 12 effective bits, absolute precision $< 1/1000$.

4.6 Metrology Light Detection at UTs

The UT IR receivers consist of an IR camera and optics each. Here, we describe the design parameters of both components. The detection will be two-fold: The first order signal will come from scatterers mounted onto the M2-spider (section 4.6.2), the higher order corrections can be derived from the image of M2. Both signals will be measured with the same cameras.

4.6.1 IR Cameras

From the physical requirements, we derive the following requirements for the IR cameras:

- The image of M2 needs to be mapped onto at least 160×160 pixels (4 pixels per fringe, 40 fringes).
- It shall be possible to observe the inner parts of the spider arms as well.
- The read noise should be below 250 electrons.
- A quantum efficiency of at least 30% at 1.9μm.
- The frame rate shall be adjustable from 10 Hz to 200 Hz.
- The dynamic range must be sufficient to allow for exposures of 40ms at least at the given thermal background.

4.6.2 Scattering Screens on Telescope Spider

The IR cameras will also be used to image the (inner parts of the) spider arms on which M2 is mounted. Optically, these arms are in the M1 space. The metrology light gets reflected via M2 and M1 into the direction of the two celestial objects that are being observed with GRAVITY. This light also shines on the spider arms from below. Hence, having a fix reference point on the spider arms at which the ABCD algorithm can be observed with the cameras is a suitable realization of the requirement that the metrology signal shall be measured in M1 space (Lacour et al.[4] 2010). The fixed reference points can be optimized to be good scatterers to ease detection of the signal. The scattering screens on the telescope spider shall fulfill the following requirements:

- Size: smaller than 1/4 of a fringe. Given the diameter of M1 (8m), the maximum number of fringes (40), this means the scatterers shall not exceed 5 cm in diameter.
- The scatterers shall be completely passive devices with a high scattering strength (the albedo shall be larger than 80%).
- The scatterers shall be suitable for detection with an external metrology, i.e. they should carry clearly visible optical targets.

Our current baseline design consists of 4 little metal cubes with dimensions of 20×20 mm. The surface pointing downwards has a matte white color; the four surfaces pointing to the sides contain optical targets. The scatterers will be screwed onto the spider arms in a position that is

- close enough to M2, such that it is inside the field of view of the cameras
- not too close to M2, such that no excess metrology light from the beam going from M3 to M2 and shining beyond M2 perturbs the signal of the metrology light traveling via M1.
- not too close to M2, such that none of the 4 scatterers will be shadowed by the M2 body, i.e. all are visible from the IR cameras.

4.7 Metrology Light Detection at ATs

The metrology fringes at the ATs will be sampled by four IR sensitive photo diodes mounted on the four spider arms which hold the M3 mirror. In order to increase the effective area of the diodes without increasing their noise, the metrology light is focused by a lens of 10 mm diameter onto the diode. A pre-amplifier will be placed right next to the diode and the amplified and low-pass filtered analog signal will be transported to the Nasmyth electronics box. There the four analog signals of the four diodes will be sent via a digital fiber link using the pre-installed single mode fibers to all AT stations to the central Combined Coudé lab and converted back to an analog signal. In the Combined Coudé lab the 16 analog signals from the four diodes at the four ATs will be directly digitized by the metrology real-time computer (see section 5).

The metrology fringes detection and read-out on the ATs consists of the following components:

- 4 photodiodes on M3 spider + pre-amplifier (max 1 W power consumption) per AT
- analog optical link between AT stations and Combined Coudé lab
- ADC.

The IR sensitive diodes, amplifiers and the ADCs shall fulfill the same requirements as the respective components of the metrology calibration sensor diodes, see section 4.5.

5. COMPUTING / SLOW CONTROL

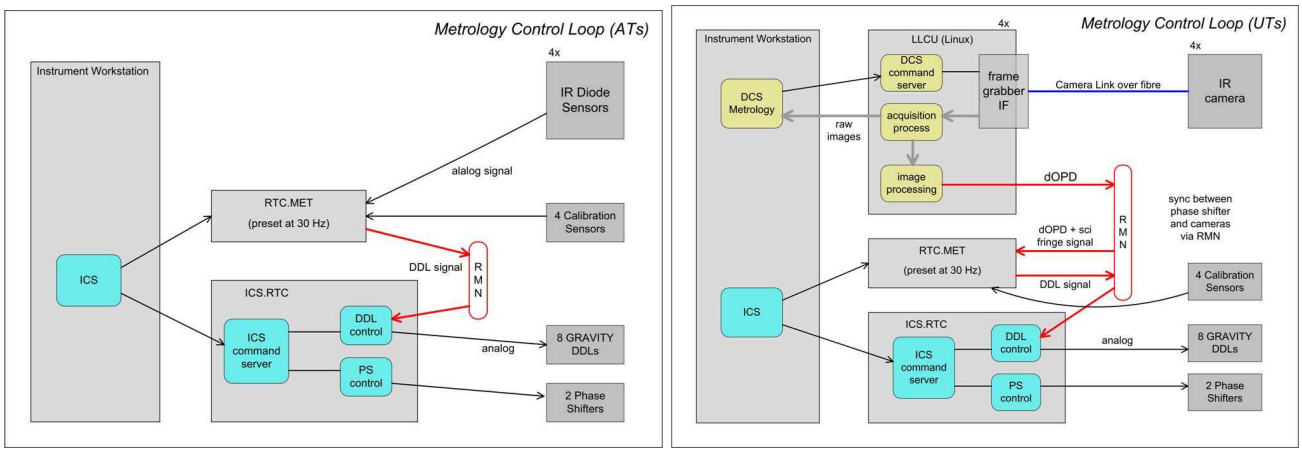

Figure 3. Left: Metrology computing block diagram for the case of ATs. The RTC.MET and ICS.RTC computers are located in the Combined Coudé lab and the IR diodes are located on the M3 spiders of the ATs. The calibration sensors, DDLs and phase shifters will be located inside the GRAVITY cryostat in the VLTI lab. Right: Metrology computing block diagram for the case of UTs. The LLCU, RTC.MET and ICS.RTC computers are located in the Combined Coudé lab and the IR cameras are located on the UTs. The calibration sensors, DDLs and phase shifters will be located inside the GRAVITY cryostat in the VLTI lab.

The metrology system employs the phase shifting interferometer ABCD algorithm (see section 3.2) to measure the path difference between one telescope and the two beam combiners. This requires an accurate timing between the phase shifter, the metrology calibration sensor diode and the metrology fringe detectors at the UTs and ATs. The 30 Hz phase shifting is steered by the metrology real-time local control unit (RTC.MET LCU). This computer is synchronized via the ESO reflective memory network (RMN, see Wallander, A.[14] 2006) with the instrument control system real-time control unit (ICS.RTC LCU), which steers the eight DDLs and the two metrology phase shifters. In the final design phase, we will evaluate whether the DDLs and phase shifters may also be steered by the RTC.MET LCU reducing the complexity of the system. The analog signals of the metrology calibration sensors and the IR sensitive diodes of the ATs are recorded directly in the RTC.MET LCU. The IR cameras

of the UTs are controlled by a dedicated real time Linux based local control unit (LLCU), which is connected to the RTC.MET via the RMN. Figure 3 (left) shows the layout of the Metrology Control Loop for the case of ATs. Figure 3 (right) shows the layout of the Metrology Control Loop for the case of UTs. The raw images of the metrology cameras are sent directly from the LLCU (including appropriate time stamp) to the instrument workstation for data storage.

5.1 Data Inputs / Outputs

Table 1 shows the science data inputs, their rate and number of bits. All of these data have to be stored including an accurate time stamp for offline analysis. The data rate is dominated by the pictures of the IR cameras of the UTs. There are only two real-time data outputs to steer the phase shifters, 14 bits each at a rate of 30Hz.

Name	rate / Hz	# bits
laser power	1	12
laser wavelength	1	12
laser status	1	8
4× metrology calibration sensor (12 bits each)	1000	48
4× UT IR cameras (256 × 256 pixels, 14 bit)	30	4E+06
4×4 AT IR diodes (12 bits each)	1000	3072

Table 1. Science data inputs, their rate and number of bits.

5.2 Real-Time Computation Tasks

The following real-time computation tasks are necessary for the GRAVITY metrology system:

- on the LLCU:
  - IR camera Image Acquisition Process software
  - Metrology Phase Analyzer software
- on the RTC.MET:
  - DDL Signal Processor software
  - metrology calibration sensor read-out software
  - AT fringe sampling diodes read-out software
- on the ICS.RTC:
  - DDL Controller software
  - metrology phase shifter controller software.

5.3 Data Storage

We plan to store the full metrology raw data in order to be able to do a detailed offline analysis. The amount of data to be stored is dominated by the image size of the metrology cameras. To reduce the data stream to be archived, 40 successive metrology camera raw frames will always be integrated (co-added) into four frames corresponding to the phase shifter settings A, B, C, and D, which will then be stored, resulting in a data stream of 480 kB/s.

6. CALIBRATION STRATEGY AND PERFORMANCE

Here we shortly present the calibration strategy and performance of the GRAVITY metrology and its subcomponents.

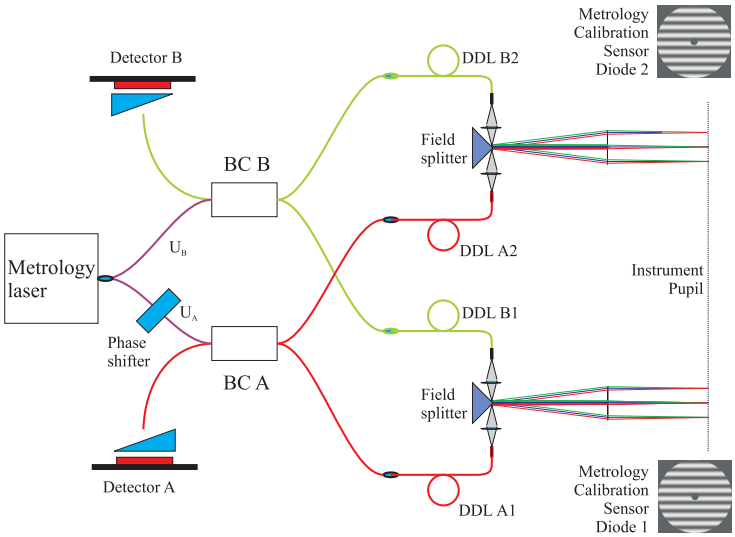

Figure 4. Metrology optical path from the IR laser to the Metrology Calibration Sensor Diode, which samples the interference pattern of the metrology laser light tracing the path of the two stars A and B behind the dichroic in the GRAVITY fiber coupler.

6.1 Metrology Calibration Sensor Diode

The light intensity at the metrology calibration sensor diode 1 mounted in the pupil center is (see figure 4):

$$\Phi_1 = \{(DL_{B1} + U_B) - (DL_{A1} + U_A)\} \frac{2\pi}{\lambda_L} + \alpha(V) \ , \tag{8}$$

where $\alpha(V)$ denotes the phase shift of the phase shifter device according to the control voltage V. Therefore, the metrology calibration sensor allows to:

- monitor the metrology IR laser power
- adjust/monitor the metrology fiber positioner
- in-situ calibrate the phase shifter
- calibrate the DDL, monitor the DDL position.

For a fixed position of the metrology fiber positioners as well as phase shifter and DDL settings the observed intensity with the metrology calibration sensor diode is proportional to the power of the metrology laser.

6.1.1 Performance of Metrology Calibration Sensor Diode

According to the metrology transmission budget (see table 2), we expect an intensity of 18 mW in the pupil of the fiber coupler. The center of the 18 mm diameter pupil will be sampled with a fiber of 100 μm core diameter. The fiber diameter corresponds to 1/4 of the fringe spacing of max. 40 fringes over the pupil (18mm/40/4 = 112 μm). The light power in the fiber is thus (including a transmission of the dichroic of 1%): $I_{\text{fiber}} = 5.6{\cdot}10^{-9}$ W. Accounting for possible losses in the multimode fiber and the coupling between fiber and metrology calibration sensor photodiode, we expect a light flux on the diode of $I_A + I_B = 5 \cdot 10^{-9}$ W. The average intensity over one ABCD phase shift cycle is then $\langle I_A + I_B \rangle = 2.5 \cdot 10^{-9}$ W. According to the specifications (see section 4.5) the error of the intensity measurement is dominated by the noise of the amplifier of $< 3 \cdot 10^{-12}$ A/Hz$^{1/2}$. Together with a response of the diode of 1 A/W this results in a noise equivalent power per 33 ms exposure (phase shifter time step) of NEP$= 1.7 \cdot 10^{-11}$W. According to equation 11 the phase error $\Delta\phi$ per 33 ms exposure (calculated from the last 4 ABCD measurements) is $\Delta\phi = 4.3 \cdot 10^{-3} = 1.5$ nm$\frac{2\pi}{\lambda_L}$.

6.1.2 Phase Shifter Calibration

Using the GRAVITY metrology as a phase shifting interferometer (see section 5.2) relies on the phase shifts $\alpha_i = 0, \pi/2, \pi, 3\pi/2$ being exactly known. Errors in α_i will result in a systematic error of the calculated phases. The systematic phase offset will be of the same order of magnitude as the error on α_i. Since we want to measure the phase with the metrology system to 1 nm$\sim \lambda/2000$, the individual phase shifts have to be known to at least the same level of accuracy or better. The calibration routine for the phase shifter developed for this purpose makes use of similar identities as shown by Rabien et al.[15] (2006), see also Rabien et al.[3] (2008).

The method described there requires a linear response of the metrology calibration sensor diode (see section 4.5). The phase shifter response function does not need to be linear. Moreover, the interferometer needs to be stable during one set of phase shift measurements, e.g. that the internal dOPD does not drift within a $\lambda/2000$ margin. Since it is possible to measure such datasets fast, this is not considered to be problematic. For phase shifts of $\alpha_2 - \alpha_1 \sim 90°$ the error of the phase shift is given by:

$$\Delta(\alpha_2 - \alpha_1) \sim \frac{\Delta I}{I} \sim 1.8 \text{ nm} \frac{2\pi}{\lambda_L} \, . \tag{9}$$

The ultimate precision of the phase shifter calibration is thus given by the number of effective bits for the D/A converter generating the phase shifter voltage. 13 effective bits (see section 4.5) correspond to 0.23 nm $2\pi/\lambda_L$. This calibration precision is reached after about 60 voltage sweeps. For an experimental test see Rabien et al.[3] (2008).

6.1.3 DDL Monitoring / Calibration

The measured phase difference with the metrology calibration sensor diode is given in equation 8. For fixed DDL_{B1} settings the observed phase shift is only a function of DDL_{A1} and the phase shifter setting (and vice versa). By applying phase shifts $\alpha_i = 0, \pi/2, \pi, 3\pi/2$ one can use the ABCD algorithm to measure changes in the DDL_{B1} length.

6.2 Metrology Zero-Point Calibration

The strategy for the metrology zero-point calibration is to observe two nearby bright stars and to swap the two stars from beam combiner A to B and vice versa. In the first calibration step we observe the two stars and obtain the following measurements: $\Psi_{A,\text{cal}}, \Psi_{B,\text{cal}}, \Phi_{1,\text{cal}}, \Phi_{2,\text{cal}}$. We then swap the two stars from one beam combiner to the other one. During this step we record the change in the metrology phases, $\Delta\Phi^{\text{swap}}_{1,\text{cal}}$ and $\Delta\Phi^{\text{swap}}_{2,\text{cal}}$. Combining these eight measurements and using equation 4, we get:

$$\Delta_1 - \Delta_2 = \Phi_{1,\text{cal}} - \Phi_{2,\text{cal}} + \frac{1}{2}\left(\Delta\Phi^{\text{swap}}_{1,\text{cal}} - \Delta\Phi^{\text{swap}}_{2,\text{cal}}\right) - \frac{1}{2}\left(\Psi_{A,\text{cal}} + \Psi^{\text{swap}}_{A,\text{cal}} - \Psi_{B,\text{cal}} - \Psi^{\text{swap}}_{B,\text{cal}}\right)\frac{\lambda_s}{\lambda_L} \, . \tag{10}$$

6.3 Metrology Polarization Adjustment

The whole optical chain from the IR metrology laser to the metrology fiber positioner is designed with polarization maintaining fibers. The polarization axis is adjusted to the key of the FC connectors to within 2°. Also the rotational fiber alignment in the fiber adapter of the fiber positioner will be done with a maximum tolerance of 2°. The metrology laser light will be injected with a high degree of linear polarization along the slow axis of the IO. In the full GRAVITY setup there will be eight fibered polarization rotators in front of the IO, see Perrin et al.[10] (2010), one for each of the two stars times four telescopes. Adjusting the fibered polarization controllers in front of the IO for maximum fringe contrast on the science targets needs six degrees of freedom of the eight rotators. A seventh degree of freedom is sufficient to adjust the relative polarization between the two stars yielding maximum fringe contrast of the metrology light at the telescope.

7. SYSTEM PERFORMANCE

In this section we will evaluate the performance expected for the GRAVITY metrology system based on the above preliminary design. We will address the following points: transmission budget, DDL control loop stability, and phase extraction performance.

#	Name	T[%] 1.9μm	Δ T BC A/B T[%]	Reference
1	vacuum feed-through, splitters, patch-cords	0.75	0.95 / 1.05	
2	phase shifter	0.7	1/1	section 4.4
3	1908nm / K band dichroic	0.98	1/1	[7,8]
4	laser-IO mode fitting / centering	0.9	0.99/1.01	[8]
5	Fresnel losses, scattering, transmission of lenses	0.9	1/1	[8]
6	IO 50/50 coupler backward propagation	0.5	1/1	[9]
7	IO 66/33 coupler backward propagation	0.33	1/1	[9]
8	IO bulk transmission	0.7	0.99/1.01	[9]
9	IO-fiber mode fitting / centering	0.93	0.98/1.02	[9]
10	glue transmission	0.99	1/1	[9]
11	fibers and fiber control	0.9	0.98/1.02	[10]
12	end face fiber #1, coated	0.99	1/1	[10]
13	fiber coupler	0.81	0.99/1.01	[11]
14	VLTI Transmission (UT DF)	0.28	1/1	[16]
	Total	0.009	0.87/1.13	

Table 2. Transmission budget from the IR metrology laser to the telescope.

7.1 Transmission and Contrast Budget

For the analysis of the performance of the metrology system the transmission budget from the IR metrology laser to the telescope is of special importance, see table 2. For a 2 W metrology laser, the total intensity (two beams) at the UT is 4.5 mW. According to Gitton[16] (2010) the VLTI transmission in the AT DF case is less (18%) resulting in a laser power of 2.9 mW at the AT. In case of on-axis observations, half of the science light is used for the AO (see Gillessen et al.[1] 2010), such that only half of the metrology light power can be observed on M2, 2.25mW.

The contrast of the metrology laser fringes at the telescopes is determined by three effects:

1. power differences (0.87/1.13) between the laser light from beam combiners A and B, see table 2.
2. contrast loss due to dOPD change caused by sky rotation during one metrology exposure (1/(30 Hz)) of max. 78 nm/s or 2.6 nm/exposure, see section 7.2
3. contrast loss due to pupil position jitter of max. 15 mm, see Pfuhl et al.[11] (2010).

These three effects result in a minimum visibility of the metrology fringe pattern in M1 space of at least 0.9, which is used in the simulations of the phase extraction performance in section 7.3.2.

7.2 DDL Control Loop Stability

The metrology signal will be used in two places: In the data reduction, it is one of the elements delivering the final phase accuracy. Online, the metrology serves as a measurement device for a control loop keeping the DDL at the required position. The accuracy by which the loop has to stay at the desired position (i.e. that the white-light fringe is matched onto the science channel) is not to be confused with the astrometric accuracy. For the loop, an accuracy of $\lambda/10$ is sufficient. This is given by the fact that the visibility loss due to the jitter in the DDL loop shall not be limiting. The loop is sketched in Figure 5. For each observation, the theoretical dOPD value as a function of time needs to be known. This is a geometrical model, the input of which is mainly the source coordinates and the wide-angle baseline. While the coordinates can be safely assumed to be known to sufficient accuracy, the requirement to be able to track the dOPD translates into a requirement on how well the baseline is known, see Lacour et al.[4] (2010). Here, the problem is to ensure that the calculated dOPD track actually is followed by the system, hence dOPD is the quantity to control. The control loop is a classical feedback system. The adjustable element is the DDL. As shown by Perrin et al.[10] (2010), the actual hardware device has a pronounced hysteresis. This is one of the reasons why dOPD needs to be controlled and a feed-forward system is not sufficient. The maximum dOPD occurring is 4 mm, for which the hysteresis reaches $0.025\% = 1\mu\text{m} \sim \lambda/2$.

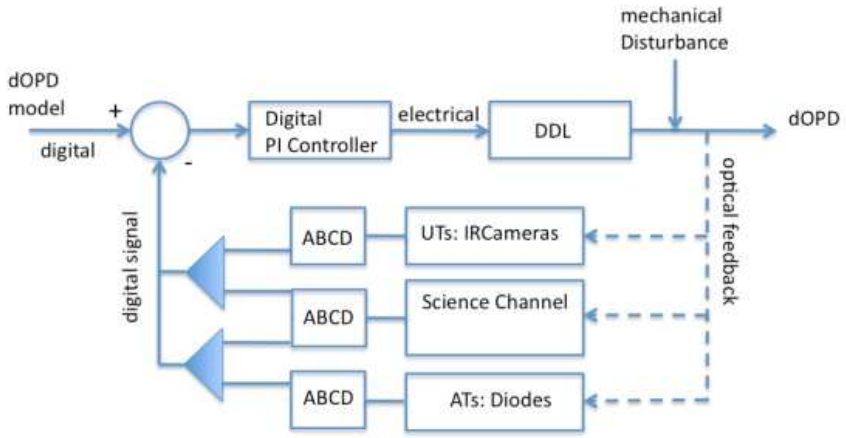

Figure 5. Basic design of the control loop for the DDL using the metrology feedback. Either the UT or AT feedback loop is used. In both cases, it might happen that the science object is bright enough to detect the white light fringe online. Then this is the most immediate feedback and should be used instead.

Even though most of the time the dOPD values will be much smaller, the design of the system should under no condition fail due to the hysteresis. The feed-back of the system is primarily optical. This means that dOPD is measured (and not the voltage applied to the DDL). Hence, the optical feedback removes the influence of the hysteresis. The actual feedback signal depends on the operation mode. For the UTs, the signal is extracted from each quadruple of ABCD images, for the ATs from a quadruple measurement of the diodes mounted on the M3 spider arm. In addition, there might be cases in which the science object is bright enough to retrieve the position of the white light fringe during the observation, e.g. when observing bright enough binaries. Then this is the ideal feedback system. Hence, either the metrology signal or even the actual science signal can be used to close the loop. For the sake of loop stability we do not foresee having a mixed sensing mode, meaning that the decision which feedback signal to use is an either-or decision at the beginning of an observation. The loop rate is given by the speed at which the metrology delivers its signal, i.e. 30 Hz. This means that the loop frequency will be in the few Hz range, i.e. the DDL loop is a relatively slow system. This is sufficient given the maximum dOPD change rates of 31 nm/s (UTs) and 78 nm/s (ATs). Assuming conservatively that the combination of OPD model and DDLs will work without feedback with a precision of 10% (for a short amount of time), the maximum deviation rate that can occur is 7.8 nm/s. Then the maximum possible deviation equals the statistical accuracy by which the phase is measured for an exposure time of 1.4 s. This will be the characteristic time scale for the control loop. This means that the dOPD is kept at all times within ± 11 nm from the nominal value (but the averaged accuracy after some minutes is much better of course).

The stability of the loop crucially depends on the accuracy of the phase measurements. The loop would break, if phase changes larger than $\pi/2$ would occur. We require that a phase error of $\pi/4$ corresponds to a statistical fluctuation of 6σ. This leads to the requirement of $\Delta\phi < \pi/4/6 = 0.13$. As shown in section 7.3 the phase accuracy is always much better than that. The loop can also monitor the phase changes it measures, which in turn allows for a health check. The stability requirement is also driving the decision whether one can track dOPD on the science object or not. This should only be done if the position of the white light fringe can be retrieved with sufficient accuracy, meaning well below $\pi/2$. Another issue is mechanical stability. The metrology system intrinsically relies on the assumption that any mechanical disturbance does not lead to phase changes larger than $\pi/2$. There is no way to recover this sort of error. It can only be recovered by tracking the dOPD with the science channel itself.

7.3 Phase Extraction Performance

The measured dOPD is the product of phase and wavelength (see section 7.4). Therefore, the phase recovery is an important contributor to the dOPD measurement.

7.3.1 Theoretical Calculations

The sensitivity of the measured phase in the ABCD algorithm to uncorrelated noise can be calculated analytically by simple error propagation:

$$\Delta\phi = \frac{1}{\sqrt{2}} \frac{\Delta I}{\langle I \rangle} \ , \tag{11}$$

where $\langle I \rangle$ is the average intensity over one ABCD cycle and ΔI is the RMS noise of one of the intensity measurements A, B, C and D.

The calculation above assumes completely uncorrelated errors as is the case for the background and read-out noise of the IR camera and IR diodes. The power output of the IR laser fluctuates with a white noise spectrum. The temporal correlation of the fluxes results in smaller phase errors than in the uncorrelated case. We have checked this explicitly by simulating white noise laser light curves. Moreover, there is a spatial correlation between the signals of the individual pixels of the IR camera. Taking an average over the whole pupil (the case of measuring via M2 on the UTs) yields virtually no phase error due to intensity noise of the laser.

We conclude, that the analytical formula 11 is correct for uncorrelated intensity fluctuation and is a conservative estimate in case of a realistic noise model.

7.3.2 UT Simulations

In order to verify the metrology system design we simulated the scattering pattern on M2 and its observation with the IR camera. In parallel, we also simulated the signals received from the scatterers. Thus, for each simulated image, we extracted two phase measurements, one based on M2 and one based on the scatterers. More specifically, the simulation parameters were:

- visibility of fringe pattern: 0.9
- object separation 1", at a random angle
- distance camera to M2 / scatterers: 9.5 m
- IR camera: 220 electrons read-noise, 35% quantum efficiency
- Exposure time: 33 ms
- optics: $f/0.9$, 71% transmission, including laser line filter for background rejection
- scatterers: (2.5×2.5) cm^2 size, albedo 0.8, scattering coefficient 2.5×10^{-4}/sr (Rabien et al.[3] 2008).

For the phase extraction, various levels of laser power (measured as total power arriving on M2, i.e. the sum of the two beams) have been investigated. If no phase information could be retrieved at all due to a too low laser power, one expects an RMS phase scatter of $2\pi/\sqrt{12}$. At a high laser power, the intensity noise of the laser is ultimately the limiting factor. For a single scatterer, the phase error due to intensity noise is given by equation 11, while for the measurement via M2, the intensity noise averages out since at each point in time many pixels sample the full fringe pattern. In order to illustrate this, we have included an artificially high intensity noise in the simulation. In the regime in-between, one expects that the phase error diminishes with $1/\sqrt{\mathrm{SNR}}$. Thus, for each power level, we generated a set of 100 ABCD sequences and for each cycle extracted the phase in two ways. By taking the average and RMS of each set, we were able to measure the accuracy of the algorithm. The final compilation of phase error versus laser power is shown in Figure 6. It fully confirms the theoretically expected behavior at the low and high flux end.

The chosen design yields total laser powers on M2 of 4.5mW (off-axis AO case) and 2.25mW (on-axis AO case) for UT observations, see table 2. This corresponds to phase uncertainties per ABCD cycle of 0.025 rad and 0.05 rad. A phase error of 0.13 rad (see section 7.2) corresponds to a total laser power of 1 mW. This is a hard limit below which the GRAVITY system would not work reliably.

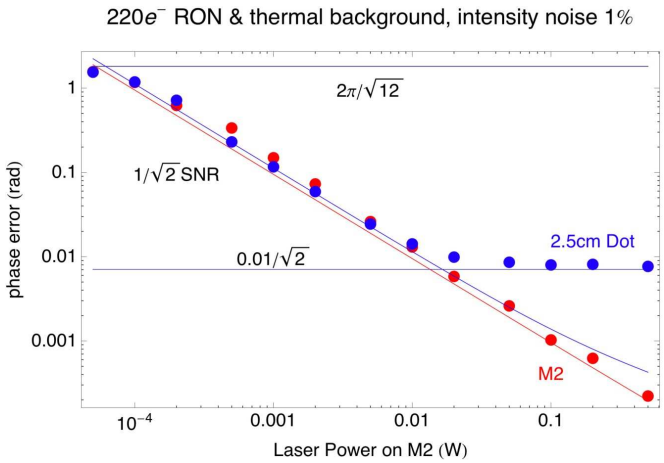

Figure 6. Phase error as a function of (total) laser power on M2. The blue dots are for the phase signal extracted from the scatterers. The red dots use the image on M2. At low fluxes, the phase error reaches asymptotically the value of a flat distribution. At high fluxes, the signal from a single scatterer is dominated by the intensity noise, which here was chosen for illustrative purpose to be artificially high with 1%. The regime in which the GRAVITY metrology will work at 4.5 mW, leading to a phase error of 0.025 rad.

7.3.3 AT Performance

A field of view of 8" corresponds to 40 fringes of the metrology laser light. A full fringe is 50 mm wide on the 2 m diameter mirror M1. According to table 2 the total power of the metrology laser (two beams, red and green) at the telescope is 2.9 mW. According to section 4.5 we sample the fringe with an aperture of 10 mm diameter. Therefore, we expect a flux on the diode of: $I_A + I_B = 7.2 \cdot 10^{-8}$ W. The average intensity over one ABCD phase shift cycle is then $\langle I_A + I_B \rangle = 1/2(I_A + I_B) = 3.6 \cdot 10^{-8}$ W . According to the specifications (see section 4.5) the error of the intensity measurement is dominated by the noise of the amplifier of $< 3 \cdot 10^{-12}$ A/Hz$^{1/2}$. Together with a response of the diode of 1 A/W this results in a noise equivalent power per 33 ms exposure (phase shifter time step) of NEP$= 1.7 \cdot 10^{-11}$ W.

According to equation 11 the statistical phase error $\Delta\phi$ per 33 ms exposure (calculated from the last 4 ABCD measurements) is given by:

$$\Delta\phi = \frac{1}{\sqrt{2}} \frac{\text{NEP}}{\langle I_A + I_B \rangle} = 3.4 \cdot 10^{-4} = 0.11 \text{ nm} \frac{2\pi}{\lambda_L} \ . \tag{12}$$

Therefore, the total uncertainty of the phase measurement will rather be dominated by the uncertainties in the phase shifter calibration and other systematic effects due to a sampling of the fringe pattern in the pupil as compared to the case of the UTs, where the full pupil image can be analyzed.

7.4 Differential OPD Extraction Performance Budget

The performance of the instrumental differential OPD measurement is subject to the error contributions outlined in table 3. The metrology system fulfills the performance requirement (section 2.1) of a phase measurement within 3 minutes to an accuracy of 1 nm. The performance of the metrology system is dominated by systematic effects like precision of measurement equipment and calibration stability.

8. CONCLUSIONS AND OUTLOOK

In this document we have presented the preliminary design of a metrology system for the GRAVITY instrument. We have shown that the presented preliminary design fulfills the physical requirements. With this preliminary system design we can measure the differential phase between the two-object beam paths with 1 nm accuracy in only 3 minutes. Systematic errors are widely excluded, due to the mapping of the full pupil over the full VLTI and telescope beam train. We have defined detailed requirements for each sub-component of the metrology system.

#	Phase error contribution	value	Phase error 3 min, 2", UT	Phase error 3 min, 2", AT
1	wavelength uncertainty IR laser	< 30 MHz	< 0.21 nm	< 0.78 nm
2	intensity noise IR laser	$< 0.5\%$ per 33 ms	< 0.04 nm	< 0.04 nm
3	phase shifter amplitude modulation	$< 0.5\%$ per 33 ms	< 0.04 nm	< 0.04 nm
4	amplitude modulation IO coupling jitter	$< 0.1\%$ per 33 ms	< 0.01 nm	< 0.01 nm
5	phase shifter calibration + stability	$< \lambda/5000$	< 0.38 nm	< 0.38 nm
6	amplitude variation in VLTI train	$< 1\%$ per 33 ms	< 0.08 nm	< 0.08 nm
7	metrology zero-point calibration + stability	< 0.5 nm	< 0.5 nm	< 0.5 nm
8	metrology receiver noise (UTs)	< 0.06rad per 33 ms	< 0.5 nm	
9	metrology receiver noise (ATs)	< 0.01rad per 33 ms		< 0.11 nm
	Total		< 0.84 nm	< 1.0 nm

Table 3. dOPD measurement performance error budget for the UT and AT case.

REFERENCES

1. Gillessen, S. et al., "GRAVITY: a four telescope beam combiner instrument for the VLTI," *these proceedings* (2010).
2. Leveque, S. A. et al., "Toward nanometer accuracy laser metrology for phase-referenced interferometry with the VLTI," *SPIE Conference Series* **4838**, 983–994 (2003).
3. Rabien, S. et al., "Fringe detection laser metrology for differential astrometric stellar interferometers," *SPIE Conference Series* **7013**, 16 (2008).
4. Lacour, S. et al., "Baseline definitions for the astrometric mode of the GRAVITY instrument," *these proceedings* (2010).
5. Choquet, E. et al., "GRAVITY: design and performance of the fringe tracker," *these proceedings* (2010).
6. Malacara, D., [*Optical Shop Testing*], Wiley New York (1992).
7. Araujo-Hauck, C. et al., "GRAVITY spectrometer: metrology laser blocking strategy at OD=12," *these proceedings* (2010).
8. Straubmeier, C. et al., "The GRAVITY spectrometers: optical design and principle of operation," *these proceedings* (2010).
9. Jocou, L. et al., "Development of the integrated optics beam combiner assembly for GRAVITY/VLTI," *these proceedings* (2010).
10. Perrin, G. et al., "Fibered optical functions for GRAVITY," *these proceedings* (2010).
11. Pfuhl, O. et al., "The fiber coupler subsystem of the future VLTI instrument GRAVITY," *these proceedings* (2010).
12. Leviton, D. B. and Frey, B. J., "Temperature-dependent absolute refractive index measurements of synthetic fused silica," **6273**, 78 (2006).
13. Dangui, V. et al., "Phase sensitivity to temperature of the fundamental mode in air-guiding photonic-bandgap fibers," *Optics Express* **13**, 6669 (2005).
14. Wallander, A., [*Interface Control Document between VLTI Supervisor Software and VLTI Intrumentation Software*] (2006). VLT-ICD-ESO-15410-2117.
15. Rabien, S. et al., "Atmospheric turbulence compensation with laser phase shifting interferometry," *A&A* **450**, 415–425 (2006).
16. Gitton, P., [*VLT Interface Control Document between VLTI and its Instruments*] (2010). VLT-ICD-ESO-15000-4809.